Lattice dynamics of the fluoride scheelite $CaZnF_4$

2000 J. Phys.: Condens. Matter 12 7395

(http://iopscience.iop.org/0953-8984/12/33/307)

J. Phys.: Condens. Matter **12** (2000) 7395–7408. Printed in the UK PII: S0953-8984(00)06493-6

Lattice dynamics of the fluoride scheelite $CaZnF_4$

S Salaün†§, A Bulou†, J Y Gesland† and P Simon‡

† Laboratoire de Physique de l'État Condensé, Faculté des Sciences, Université du Maine, Avenue O Messiaen, 72085 Le Mans Cédex 9, France
‡ Centre de Recherches sur les Matériaux Haute Température 1D, Avenues de la Recherche Scientifique, 45071 Orléans Cédex 2, France

Received 30 July 1999, in final form 13 March 2000

Abstract. The lattice dynamics of the fluoride scheelite $CaZnF_4$ have been investigated by means of infrared reflectivity and Raman scattering. The measured phonon modes have been assigned to the various irreducible representations of the point group of the crystal. The phonon dispersion curves, density of states and sound velocities have been calculated within a rigid-ion model based on experimental zone-centre phonons.

1. Introduction

Fluoride compounds of scheelite structure are generally optically transparent insulators and are of considerable interest in laser optical studies [1], for example $LiYF_4$. $CaZnF_4$ is one of the most recent fluoride isomorphic compounds that has been synthesized [2], and could, like other isomorphs, be used for optical applications. Its particular interest, among the fluoride scheelites, lies in the oxidation degrees of the cations, namely +II/+II for $CaZnF_4$, while it is +I/+III for a typical $LiLnF_4$ compound. This could highly influence the lattice dynamics of the crystal and the optical properties of a doped sample. One may indeed envisage a different doping of this particular compound i.e. with transition metal ions or divalent rare-earth ions, very different from the generally used trivalent rare-earth ions (Nd^{3+}, Eu^{3+}, ...), which could lead to new optical properties. Moreover, some of oxide scheelites, namely $BiVO_4$ and $LaNbO_4$, undergo pseudo-proper ferroelastic phase transitions ([3] and references therein). The dynamical study of the isomorphic compound $CaZnF_4$, coming after the study of the reference compound $LiYF_4$ [4, 5], could help to model this very particular type of phase transition in bringing information about the influence of oxidation degrees on lattice dynamics in this structure. In the present work, we measured zone centre phonons (infrared and Raman active) and deduced some important frequency dependent functions. We also realized lattice dynamical calculations within a rigid-ion model previously used in [5] for the isomorphic compound $LiYF_4$, this laser-matrix being here considered as a reference because of the great deal of work already performed on it in the framework of lattice dynamics.

§ Permanent address: Laboratoire de Physique de l'Université de Bourgogne, UMR CNRS No 5027, Faculté des Sciences Mirande, 9 avenue A Savary, BP 47870, 21078 Dijon Cédex, France.

0953-8984/00/337395+14$30.00

2. Structure and dynamics

As already mentioned, $CaZnF_4$ crystallizes with the same structure as the typical $LiLnF_4$ compounds, lithium and lanthanide (Ln) ions being replaced by zinc and calcium respectively. The unit cell (see [6]) is body-centred tetragonal and belongs to the $I4_1/a$ (C_{4h}^6) space group. The crystallographic parameters given in the literature ($a = b = 5.279$ Å and $c = 11.021$ Å [2]) are of the same order of magnitude as in $LiLnF_4$ compounds [6].

The elementary cell contains two formula units; the group theory analysis shows that, at the Brillouin zone centre, the 36 normal modes are distributed among the various irreducible representations of the C_{4h} factor group as follows [7]:

$$\Gamma^{vib} = 3A_g + 5B_g + 5E_g + 5A_u + 3B_u + 5E_u. \tag{1}$$

B_u phonons are neither Raman nor infrared active. The acoustic modes have A_u and E_u symmetries; the other four A_u and E_u modes are infrared active with dipole moment respectively parallel and perpendicular to the fourfold axis c. All of the 13 g-type modes are Raman active. Note that throughout this work zone-centre phonons will be sorted out by increasing wavenumber within each symmetry.

A single crystal of $CaZnF_4$, large enough for optical experiments, has been grown using the Czochralski technique. The sample, Laue x-ray oriented, has been cut perpendicularly to the three crystallographic axes a, b and c; relevant faces (polished for a good optical quality) are respectively $4 \times 4 \times 6$ mm^3 in size. It must be noted that, like the oxide scheelites but unlike fluoride ones, $CaZnF_4$ presents an easy cleaving direction, perpendicular to the fourfold axis c. Moreover, the crystal growth of this compound is, at present, much more delicate than the synthesis of other isomorphic compounds: we have not yet been able to produce larger single crystals.

3. Experimental results

3.1. Raman scattering

Following Porto and Scott [8], a scattering geometry will be described by the notation $e_1(n_1n_2)e_2$ where e_i identifies the propagation direction of laser light, polarized along n_i, e and n being X, Y or Z, which directions are respectively parallel to the crystalline axes a, b and c; the subscripts $i = 1$ and 2 refer to incident and scattered beams respectively.

Low- and high-temperature polarized Raman spectra were recorded with a DILOR Z24 triple monochromator, equipped with a cooled photomultiplier. A Leybold cryogenerator was used to obtain low temperatures. The experiments were performed, for every scattering geometry, with an excitation wavelength at 514.5 nm, slit-widths of 250 μm (spectral resolution 2.5 cm^{-1}) and a laser power of 400 mW. We present in figure 1 the spectra we obtained at about 10 K with the adapted polarization schemes to observe the modes with A_g, B_g and E_g symmetries. Table 1 lists the frequencies of the observed Raman-active phonons at low and high temperature, assigned to the various irreducible representations of the C_{4h} factor group. The number of observed modes is in agreement with the predictions of group theory and the phonon frequencies appear to be weakly temperature dependent between 300 K and 10 K.

For comparison, we also reported in table 1 the results previously obtained in the isomorphic compound $LiYF_4$ [4]: the Raman-active frequencies in $CaZnF_4$, except the highest one of each symmetry A_g, B_g and E_g, are lower than those of $LiYF_4$.

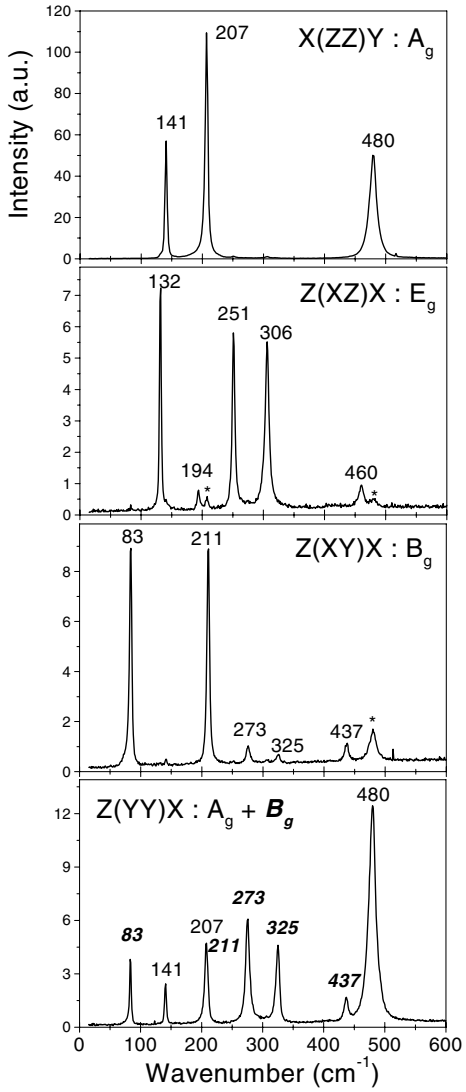

Figure 1. Raman spectra of $CaZnF_4$ at 10 K. The symmetry of the Raman-active modes is recalled for each scattering geometry. Stars indicate peaks that have been attributed to contamination by an intense line active in another geometry.

3.2. Infrared reflectivity measurements

As already mentioned (see equation (1)), there are eight polar vibration modes, infrared active, in the scheelite structure, namely four polarized parallel to the optical axis c (A_u modes), and four polarised perpendicularly to c (E_u modes). Room temperature polarized reflection spectra were recorded with a Fourier-transform rapid-scan interferometer (Bruker IFS 113V) in the spectral range [50, 6000 cm^{-1}]. The incident beam's electric vector was either perpendicular or parallel to the fourfold axis; the corresponding experimental points have been reported in figure 2 (full circles). As predicted by the group-theory analysis, they show four bands for each polarization, between 100 and 600 cm^{-1}.

Table 1. Low- and high-temperature experimental wave-numbers (in cm^{-1}) of the Raman-active phonons in $CaZnF_4$ assigned to the various irreducible representations of the C_{4h} point group. The values obtained in the reference compound $LiYF_4$ [4] are also recalled.

Mode symmetry, configuration	$CaZnF_4$ 300 K	$CaZnF_4$ 10 K	$LiYF_4$ [4]
A_g	139	141	151
$X(Z, Z)Y$	201	207	264
	475	480	425
B_g	83	83	177
$Z(X, Y)X$	211	211	248
	271	273	329
	319	325	382
	435	437	427
E_g	129	132	153
$Z(X, Z)X$	193	194	199
	247	251	329
	301	306	368
	455	460	446

As previously done for $LiLnF_4$ compounds (Ln = Ho, Er, Tm, Yb; Y) [4], the polarized experimental IR reflection spectra have been analysed through a dielectric function model to obtain the mode frequencies and dampings.

The measured reflectivity $R(\omega)$ of a material depends on the dielectric permittivity via the Fresnel formula in normal incidence:

$$R(\omega) = \left| \frac{\sqrt{\varepsilon(\omega)} - 1}{\sqrt{\varepsilon(\omega)} + 1} \right|^2 . \tag{2}$$

The 'four parameter model' develops the factorized form of the dielectric function ε [9], and is convenient to represent even asymmetrical and wide bands; it implies for each spectrum in this structure four damped oscillators, each of them representing an optical mode:

$$\varepsilon(\omega) = \varepsilon' - \mathrm{i}\varepsilon'' = \varepsilon_\infty \prod_{j=1}^{4} \frac{\Omega_{j,LO}^2 - \omega^2 + \mathrm{i}\gamma_{j,LO}\omega}{\Omega_{j,TO}^2 - \omega^2 + \mathrm{i}\gamma_{j,TO}\omega}. \tag{3}$$

The four parameters that correspond to the jth optical mode are the longitudinal $\Omega_{j,LO}$ and transversal $\Omega_{j,LO}$ angular frequencies, and the corresponding dampings $\gamma_{j,LO}$ and $\gamma_{j,TO}$. The jth bandwidth corresponds to the damping factor γ_j while transverse- and longitudinal-mode profiles are given by the imaginary part of the dielectric and inverse dielectric functions.

The high-limit value ε_∞ of the dielectric function has been deduced from the optical refraction index ($n = \sqrt{\varepsilon_\infty}$). Insofar as $CaZnF_4$ belongs to a tetragonal space group ($n_x = n_y = n_o \neq n_z = n_e$), we used the ordinary optical index n_o (respectively extraordinary: n_e) for spectra recorded perpendicularly (respectively parallel) to the optical axis. These optical indices have been determined with a Pulfrich refractometer.

Table 2 lists the frequencies of LO and TO modes used to obtain the best fit reflectivity curves (full curves in figure 2) which are in good agreement with experimental points (circles). Typically, LO and TO frequencies are determined to better than 2 cm^{-1}. As previously done for the Raman-active modes, we also report in table 2 the frequencies of the IR-active modes in the reference compound $LiYF_4$ [4]. We may observe here that the $CaZnF_4$ IR-active frequencies, except the last TO/LO pair of both A_u and E_u symmetries, are lower than those of $LiYF_4$ as already noted for the Raman-active zone-centre phonons.

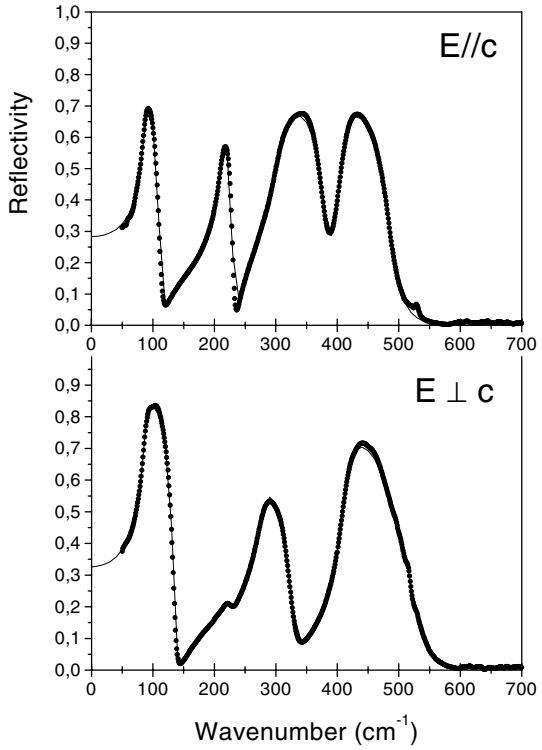

Figure 2. Room temperature infrared reflection spectra in $CaZnF_4$ recorded with the incident electric field parallel (upper graph) and perpendicular (lower graph) to the optical axis c. Circles are experimental points and full curves represent the result of an oscillator fit ('four parameter model'). The small anomalies near 520 cm^{-1} correspond to a spectral range of weak signal-to-noise ratio between two spectrometer beamsplitters.

Table 2. Wave-numbers (in cm^{-1}) of transverse and longitudinal infrared-active phonons deduced from IR-reflection experiments performed at room temperature in $CaZnF_4$. The corresponding values obtained in the reference compound $LiYF_4$ [4] with the same method are recalled.

IR-active mode	$CaZnF_4$	$LiYF_4$
A_u (TO/LO)	87/114	196/219
(cm^{-1})	212/231	251/278
	305/385	341/360
	400/487	370/534
E_u (TO/LO)	86/136	137/171
(cm^{-1})	225/227	294/308
	279/331	325/367
	410/526	418/560

The 'four parameters' model also enables the calculation of various frequency dependent physical quantities for both of the incident beam's polarizations. The real and imaginary optical indices $n(\omega)$ and $k(\omega)$, and the absorption coefficient $\alpha(\omega)$ $(=2\omega k(\omega)/c)$ are shown in figures 3(a) and (b) for both of the polarizations.

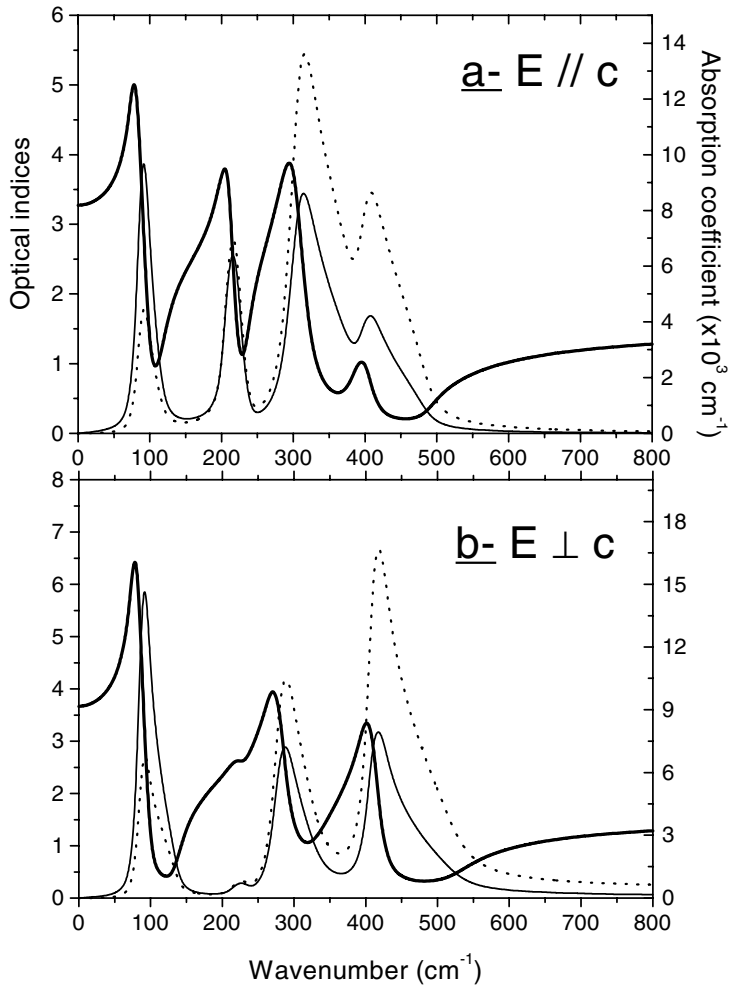

Figure 3. Calculated frequency dependent functions in $CaZnF_4$: refraction index $n(\omega)$ (bold line), extinction index $k(\omega)$ (fine line) and absorption coefficient $\alpha(\omega)$ (dotted line) in $CaZnF_4$ for $E \parallel c$ (a) and $E \perp c$ (b).

3.3. Discussion of experimental results

One can remark that, according to our experimental results, the lowest frequency zone-centre phonon in $CaZnF_4$ is B_g-type, as observed in the $BiVO_4$ isomorphic compound which undergoes a proper-ferroelastic phase transition ([3] and references therein). According to our study $CaZnF_4$ does not undergo any phase transition with temperature. We may also note that we observed the exact number of each symmetry's modes with no C_{4h} selection rule breakdown, unlike the case in oxide scheelites where B_u inactive modes have been observed consequently to strain effects [10].

Polar mode TO/LO splitting observed in the infrared measurements is rather important—except for the second modes of each of the A_u and E_u symmetries sorted out by increasing frequency—which attests to a high ionicity of bonds in this crystal. This becomes obvious if we compare the interatomic distances in the crystal (recalled in table 3, see the following

paragraph) with the sums of the ionic radii R_i in a fluorine environment listed by Kaminskii [1]:

$$d(\text{Zn–F}) = 1.931 \text{ Å} \qquad \sum R_i = 1.93 \text{ Å}$$
$$d(\text{Ca–F}) = 2.336 \text{ Å} \qquad \sum R_i = 2.33 \text{ Å}.$$

The knowledge of the whole set of TO and LO frequencies allows us to estimate the effective dynamic charges, defined by Scott [11], of all ions in the system (see [12] for review). The effective charges Ze are connected to the frequencies by

$$\sum_j (\Omega_{j,LO}^2 - \Omega_{j,TO}^2)_\alpha = \frac{1}{\varepsilon_v V} \sum_k \frac{(Ze)_{k\alpha}^2}{m_k} \tag{4}$$

where α denotes the polarization, ε_v the dielectric constant of vacuum, $(Ze)_{k\alpha}$ the effective charge along the α direction and m_k the mass of ion k. The summation is performed over all ions contained in volume V. Besides, the sum of all effective charges obviously vanishes due to the electrical neutrality. The system is then fully solved in diatomic crystals with one formula unit per elementary cell. In other systems some additional assumptions are necessary to obtain information about effective dynamic charges.

In the present case, we hence first assume that all of the fluorine ions in the elementary cell carry the same charge. The system is then reduced to three unknown parameters for two equations between them. Moreover the most important weight in the right-hand term of the above equation originates from the fluorine ion contribution, due to their lower mass and to the fact there are four fluorine ions per one calcium and zinc. An important variation of Z_{Ca} or Z_{Zn} will then induce only a small change of the fluorine charge. Z_F is therefore more precisely determined than other effective charges. Indeed our calculations yielded the following results:

- for A_u polarization, a change of the calcium reduced charge Z_{Ca} from 1.3 to 1.9 (in the physically reasonable range) corresponds to a change of Z_{Zn} from 1.87 to 1.11, but for fluorine Z_F varies only from -0.79 down to -0.75 in units of the elementary charge e;
- for E_u polarization, for the same changes in the calcium reduced charge, the variation is from 1.93 to 1.19 for zinc, and from -0.81 to -0.77 for fluorine.

The conclusion is then that in $CaZnF_4$, the fluorine reduced effective charge is very stable with regard to the cations charges and represents about 77% of the nominal charge, slightly lower along the fourfold axis than perpendicular to it.

Concerning the elastic behaviour of $CaZnF_4$, we observed that the IR- and Raman-active frequencies, except the highest frequency mode of each symmetry A_u, A_g, B_g, E_u and E_g, were lower than those of $LiYF_4$. In these conditions, because of the anticrossing phenomenon between branches of identical symmetry, we could observe different situations in comparing $CaZnF_4$ and $LiYF_4$ acoustic branches. Sound velocities (i.e. the slope of the considered acoustic branch for small wave-vector) have (i) either lower values in $CaZnF_4$ than in $LiYF_4$, which will lead to lower values of elastic constants, or (ii) similar values in both compounds, which corresponds in $CaZnF_4$ to acoustic branches linear only in a very narrow frequency range. One can discriminate between these hypotheses only with the help of further experiments (such as Brillouin scattering, ultrasonic measurements or inelastic neutron scattering), or with lattice dynamical calculations based on the available experimental results. We used here as a first approach the latter method insofar as we have already realized satisfactory lattice dynamical calculations in such an ionic fluoride scheelite compound [5].

4. Lattice dynamical modelization

To calculate the phonon spectrum of $CaZnF_4$, we used the same method and model as we did previously for the reference compound $LiYF_4$ [5]. The choice of a rigid-ion model is

Table 3. Rigid-ion model final set of parameters after fitting procedure realized on the 29 experimental infrared- and Raman-active zone centre phonons in the fluoride scheelite $CaZnF_4$. The A_i and B_i short range force constants (SRFCs, in N m^{-1}) are characteristic respectively for motions parallel and perpendicular to the line joining the atoms of the ith ionic pair (sorted by increasing interionic distance d_i). The fluorine–fluorine SRFCs (reported in bold) have been set to the values deduced from the F–F interionic potential given in [14]. The ionic effective charges (expressed in $|e|$ units) are $Z^*_F = -0.770$ (imposed), $Z^*_{Ca} = 1.50$ (and $Z^*_{Zn} = 1.58$).

i	Ions	d_i (Å)	A_i (N m^{-1})	B_i (N m^{-1})
1	Zn–F	1.931	192.8	−8.5
2	Ca–F	2.336	71.1	−8.9
3	Ca–F	2.377	68.0	−8.6
4	F–F	2.755	**12.5**	**−2.7**
5	F–F	2.767	**12.2**	**−2.6**
6	F–F	2.807	**11.4**	**−2.4**
7	Zn–F	2.808	6.7	−1.4
8	F–F	2.945	**9.0**	**−1.8**
9	F–F	3.064	**7.4**	**−1.4**

expected to be reasonable in this particular case as well insofar as calcium, zinc and fluorine have rather weak ionic polarizabilities. Moreover our purpose is here to deal with as few adjustable parameters as possible in order to compare more easily the results obtained in both compounds, and even a rough description of lattice dynamics (LD) in $CaZnF_4$ could provide physically meaningful explanations for experimental facts, such as the existence of an easy cleaving direction.

4.1. Parameters of the rigid-ion model (RIM)

Even in such a simple model [13], there are 20 independent parameters. We consider the nine shortest distances between ions, which yields 18 short-range parameters, namely nine pairs of short range force constants (A_i, B_i) which derive from axially symmetric pair potentials. The electrostatic long-range interactions are defined through three effective ionic charges $Z^*_i e$ [14], which gives only two parameters more due to the condition of charge neutrality.

The two charges Ze (Scott charge, deduced from experimental TO/LO splittings) and Z^*e (Szigetti charge, parameter of the RIM) are equal for $\varepsilon_\infty = 1$ and 4, and differ only slightly (<10%) as long as ε_∞ is lower than 6.5. In the present case, ε_∞ is close to 1 due to the small polarizability of fluorine. This allows us to use in LD calculations the well defined fluorine charge deduced from IR measurements. Moreover the anisotropy of IR-measured dynamic effective charge is small; hence an average value, namely $-0.77|e|$, is imposed for the fluorine effective charge in the rigid ion model. Insofar as cation effective charges yielded by LO–TO splitting varied a lot, we left the calcium charge free, Z_{Zn} being then imposed by charge neutrality. As previously done in $LiYF_4$ to reduce the number of adjustable parameters [4] we fixed the fluorine–fluorine short-range force constants (SRFCs) as deduced from the F–F short-range pair potential of [15].

The remaining adjustable parameters in the model are then Z_{Ca} and the eight SRFCs characteristic for Zn–F and Ca–F interactions. These nine parameters in the model have been adjusted with the help of the *GENAX2* program, implemented at the LLB (Laboratoire Léon Brillouin, Saclay, France), on the basis of the measured IR- and Raman-active frequencies, taking care of the corresponding mode symmetry.

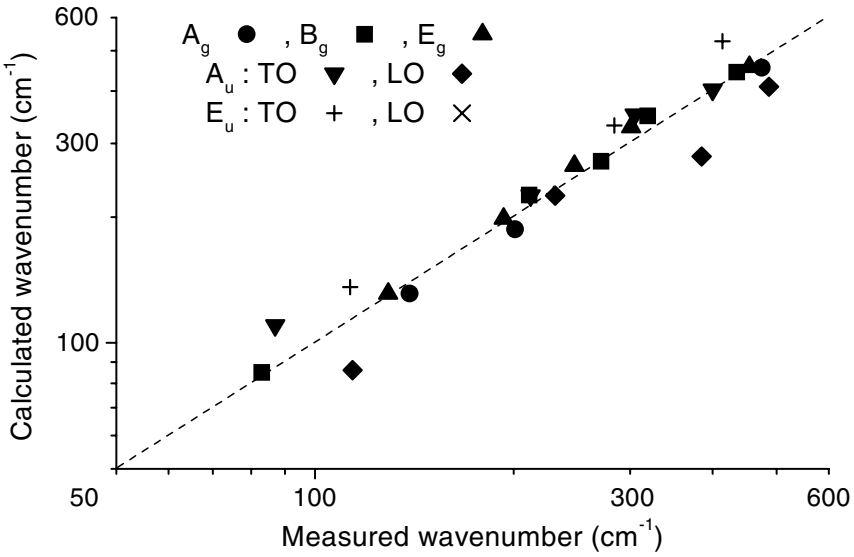

Figure 4. Comparison, in a logarithmic scale, of the calculated and experimental wave-numbers (in cm^{-1}) of the IR- or Raman-active zone-centre phonons in $CaZnF_4$. The dashed line marks equality of the two values. The average discrepancy between the 29 calculated and corresponding measured zone-centre phonons is 7.6%.

The final set of parameters is reported in table 3. With these values, the average discrepancy between the 29 calculated and measured zone centre frequencies is less than 7.7%, as shown in figure 4, which is a rather satisfying agreement insofar as only eight parameters were adjusted among 20.

All of the values of the SRFCs are smaller in $CaZnF_4$ than in $LiYF_4$ (which decreases all the frequencies) except the (A_1, B_1) pair—relative to the shortest Zn–F interaction—which is much higher than any of $LiYF_4$. The strong values of this (A_1, B_1) pair appears as a reflection of the short Zn–F distance, much smaller than the Ca–F one, in spite of the same cation valence (while in $LiYF_4$, due to the charge discrepancy—I/III—the Li–F force constants were much smaller than the Y–F ones). Indeed, if only the ion masses were involved, the highest-frequency modes of each symmetry would be higher in $LiYF_4$ than in $CaZnF_4$ (the Li atom being much lighter than any cation in $CaZnF_4$), which is not what is experimentally stated; hence the SRFCs corresponding to the shortest distance have to be much stronger in $CaZnF_4$ than in $LiYF_4$.

In addition, calculations show that the highest-frequency modes of each symmetry ($A_{g(u)}$, B_g and $E_{g(u)}$) merely depend on the (A_1, B_1) pair alone. These modes then correspond essentially to vibrations inside the ZnF_4 tetrahedra. This also explains why only the highest frequencies of each symmetry are greater in $CaZnF_4$ than in $LiYF_4$.

The A_i and B_i SRFCs relative to Zn–F pair interactions may be compared to the results obtained by other authors in different fluoride compounds, namely:

in ZnF_2 ($d_{Zn-F} \approx 2$Å):	$A_{Zn-F} \approx 142$, $B_{Zn-F} \approx -16\ N\ m^{-1}$ [16]
in K_2ZnF_2 ($d_{Zn-F} \approx 2$Å):	$A_{Zn-F} \approx 143$, $B_{Zn-F} \approx -21\ N\ m^{-1}$ [17]
in $KZnF_2$ ($d_{Zn-F} = 2.027$Å):	$A_{Zn-F} = 99.5$, $B_{Zn-F} = -12\ N\ m^{-1}$ [18]
	$A_{Zn-F} = 103.9$, $B_{Zn-F} = -14.2\ N\ m^{-1}$ [19].

The values we obtained in $CaZnF_4$ are a bit higher, in agreement with the shorter interionic distance ($d = 1.931$ Å). In addition, the ratio A_1/A_7 between identical force constants for different interionic distances is very close to the one we can deduce from the Zn–F pair-potential defined by Becher *et al* [20], and leads, in the hypothesis of a Born–Mayer type potential, to a coefficient $\rho = 0.26$ Å, as generally observed for metal/fluorine interactions.

The present investigation also shows that the experimental frequencies of each symmetry's lowest frequency mode are lower in $CaZnF_4$ than in $LiYF_4$. This witness for the fact that the SRFCs of the Ca–F interactions are much smaller than Y–F ones to compensate the mass and charge differences between Ca^{2+} and Y^{3+}—that would lead to increased frequencies when replacing Y^{3+} by Ca^{2+}. The obtained Ca–F SRFCs have the same magnitude as those determined in the calcium fluoride perovskites $CsCaF_3$ [19], $KCaF_3$ and $RbCaF_3$ [21]. Moreover, the ratios A_i/B_i for $i = 2$ and 3, and A_2/A_3 are quite identical to those deduced, with the adapted interionic distances, from the corresponding pair potentials defined by Catlow *et al* and Watson *et al* [22, 23]. Therefore the Ca–F interaction seems to derive from a Born–Mayer type potential, with a parameter $\rho \approx 0.3$ Å.

It is worth noting that, according to our calculations and for given values of the effective charges, the value of the A_3 SRFC is imposed by the frequency of the B_g-symmetry phonon measured at 271 cm^{-1} (at room temperature). This particular mode then generates a stretching of the second shortest Ca–F bonds, i.e. of half the 'double tetrahedron' CaF_8. Such a simple relation between SRFCs and a particular phonon frequency did not exist in the reference compound $LiYF_4$, where phonons generally correspond to complicated atomic motions.

4.2. Calculated phonon dispersion curves, density of states and deduced ultrasonic velocities

The dispersion curves (along the [100], [110] and [001] directions of the quadratic Brillouin zone) and the one-phonon density of states, calculated with the model described in the previous paragraph, are respectively drawn in figures 5 and 6. According to these calculations, many flat phonon branches (between 11.5 and 14 THz) are predicted in this compound unlike in $LiYF_4$, which gives rise to an intense peak around 410 cm^{-1} in the density of states curve; one may note that even inelastic neutron scattering would be relatively inoperative to measure these phonons because of the difficulties encountered with this technique at high frequencies when many modes are present in a narrow frequency range.

It appears also in figure 5 that, for lines normal to the tetragonal axis, the lowest frequency B_g mode belongs to a phonon branch (Σ_1 symmetry on ΓKZ on ΓX) that does not seem to exhibit any anticrossing with the transverse acoustic branch of the same symmetry (Σ_1 or Δ_1). So there is no sign of a coupling between optical and acoustic modes such as what occurs in the isomorph $BiVO_4$, where the softening of a B_g mode drives a pseudo-proper ferroelastic phase transition. Moreover, the present Raman scattering investigation shows no phase transition or softening of the B_g mode within the explored range of temperature (which is better for eventual optical applications). Therefore, with regard to the data currently available, $CaZnF_4$ appears as a very stable crystal.

Figure 6 also shows the partial density of states $g_i(\omega)$ (with $i =$ Zn, Ca or F), which represents the weighted contribution of the corresponding ionic species and that verifies

$$g(\omega) = g_{Zn}(\omega) + g_{Ca}(\omega) + g_F(\omega). \tag{5}$$

Several frequency intervals may then be considered:

- 0 to ~150 cm^{-1} and 400 to 415 cm^{-1} (flat branches): atomic movements mostly imply zinc and fluorine ions;

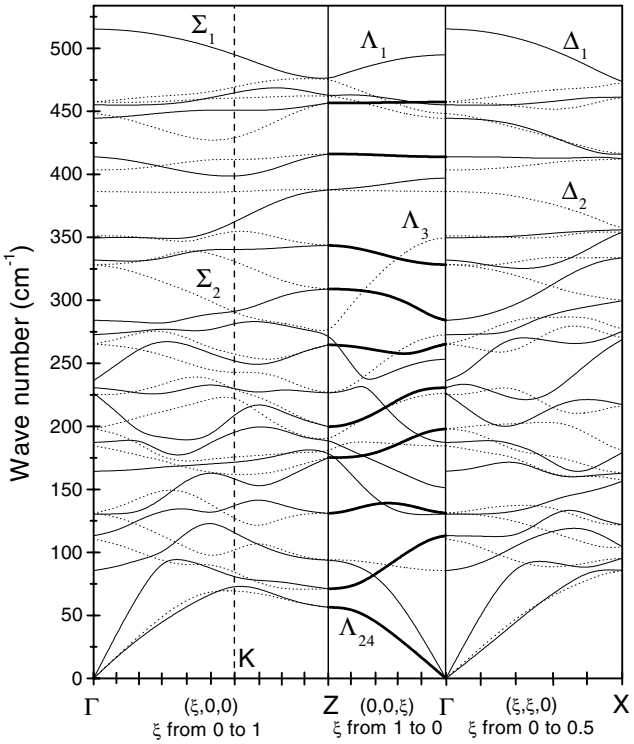

Figure 5. Phonon dispersion curves calculated with a rigid-ion model along the ΓKZ, ZΓ and ΓX lines of the Brillouin zone, with the following conventions (also reported on the graph): fine full curves for Σ_1, Δ_1 and Λ_1 branches, dotted curves for Σ_2, Λ_3 and Δ_2 symmetries and bold full curves for the—degenerate—Λ_{24} branches along the quadratic axis direction ΓZ.

- ∼200 to ∼330 cm^{-1}: in this frequency range, vibrations involve principally calcium and fluorine ions;
- ∼330 to ∼500 cm^{-1}: there are very important movements of fluorine ions, this frequency range being red-shifted when compared to the results obtained in $LiYF_4$.

In the present case, as already noted for $LiYF_4$ [5], there is no clear discrimination between internal and external modes which would respectively imply movements within and between tetrahedral MF_4 units. This ensues from the mainly ionic character of chemical bonding in fluoride compounds: quasi-molecular tetrahedral units do not exist in fluoride scheelites, contrary to what is stated in oxide isomorphs where bonding has a more important covalent character inside the tetrahedral unit [8, 10].

As shown in the inset in figure 6, the Debye law—$g(\omega) \propto \omega^2$—is valid up to 42 cm^{-1}; the corresponding wave-vector mean limit reaches almost half the shortest distance between the centre and boundary of the Brillouin zone. Considering this rather high value of Debye's limit, and the lower values of the phonon frequencies at zone boundaries and centre compared to the $LiYF_4$ case, it implies a lower slope for the acoustic branches. These slopes may be deduced directly from our calculations, yielding this way the ultrasonic velocities V (m s^{-1}) through the following relation:

$$V = 100\nu \left(\frac{1}{a^2}(\xi_1^2 + \xi_2^2) + \frac{1}{c^2}\xi_3^2 \right)^{-1/2} \tag{6}$$

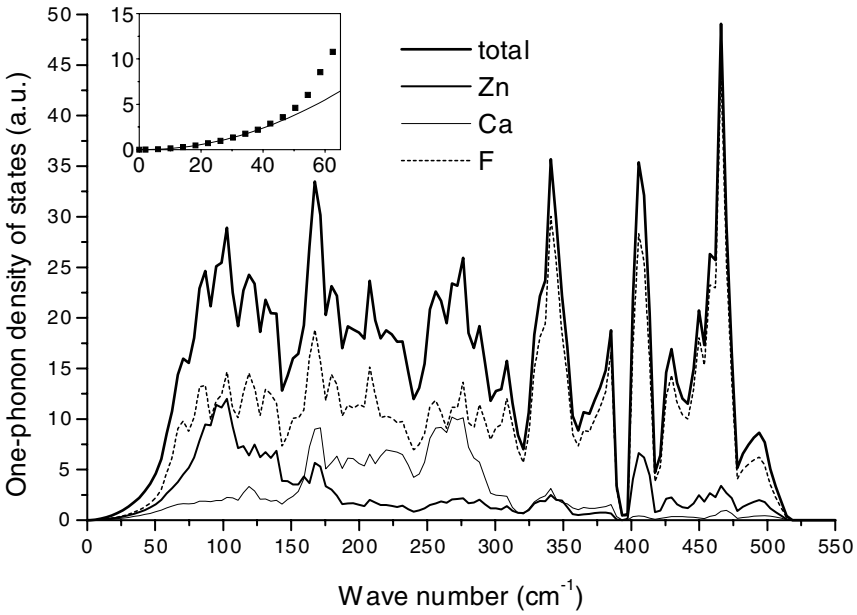

Figure 6. Normalized one-phonon density of states calculated within a rigid-ion model (with an energy step of 0.5 MeV): total and partial density of states for each atomic species with $g_{total}(\omega) = g_{Zn}(\omega) + g_{Ca}(\omega) + g_F(\omega)$. In the inset, squares represent the total density of states for the low-frequency range, and the line results from a parabolic fit from $g_{total}(\omega)$ to account for Debye's law.

Table 4. Longitudinal (L) and transverse (T) wave ultrasonic velocities V_i (in m s^{-1}) measured in the reference compound $LiYF_4$ [24], and estimated (on the basis of the calculated phonon spectrum) in $CaZnF_4$ for the highest-symmetry lines of the scheelite structure's Brillouin zone.

Propagation direction	Polarisation direction	Mode	V_i (m s^{-1}) calculated in $CaZnF_4$	V_i (m s^{-1}) measured in $LiYF_4$
[001]	[001]	L	$V_1 \approx 5400$	$V_1 = 6240$
(ΓZ line)	(001) plane	T	$V_2 \approx 2800$	$V_2 = 3200$
[100]	(001) plane	Quasi-L	$V_3 \approx 5700$	$V_3 = 5510$
(ΓKZ line)		Quasi-T	$V_4 \approx 2800$	—
	[001]	T	$V_5 \approx 2800$	$V_5 = 3210$
[110]	(001) plane	Quasi-L	$V_6 \approx 5800$	$V_6 = 5230$
(ΓX line)		Quasi-T	$V_7 \approx 2400$	$V_7 = 2700$
	[001]	T	$V_8 \approx 2800$	$V_8 = 3210$

where ν is the acoustic phonon frequency (expressed in THz) calculated for a small wave-vector, $\boldsymbol{q}$ of which the reduced coordinates are (ξ_1, ξ_2, ξ_3) in the reciprocal basis $(\boldsymbol{a}^*, \boldsymbol{b}^*, \boldsymbol{c}^*)$. In this formula, the lattice parameters a and c are given in Å.

The values of the ultrasonic velocities we obtained with this method in the three main directions ΓKZ, ZΓ and ΓX of the reciprocal lattice are reported in table 4; they may be directly compared to the ultrasonic velocities measured in $LiYF_4$ [24], all the more because both

compounds have really close values of mass per unit of volume ($CaZnF_4$: 3923 kg m^{-3} [25], $LiYF_4$: 3996 kg m^{-3} [24]). Some tendencies concerning the physical behaviour of $CaZnF_4$ can be advanced from these estimations.

Crystals with a scheelite structure have $4/m$ (TII) Laue symmetry; they show acoustic symmetry about an orthogonal axial set of which only the fourfold axis (Z) is a conventional crystallographic axis [26]. Blanchfield and Saunders reported in [24] the relationships between ultrasonic velocities and the six independent elastic constants for this kind of structure. According to those relations, and considering the experimental and calculated values reported in table 4, the elastic constants C_{33} and C_{44} would be lower in $CaZnF_4$ than in $LiYF_4$, whereas $(C_{11} + C_{66})$ would be higher. Hence $CaZnF_4$ would have greater elastic anisotropies than $LiYF_4$, which can explain the existence in the former and not in the latter compound of an easy-cleaving direction, perpendicular to the fourfold axis c.

5. Conclusion

The present results report on the first dynamical data (Raman and infrared) for $CaZnF_4$, that is an uncommon fluoride scheelite with regard to the cation valences. Investigations from room temperature to 10 K prove that this compound does not undergo any phase transition in this temperature range and so can be considered as a valuable host matrix for doping in optical applications. All of the IR- and Raman-observed modes have been assigned to the various irreducible representations of the point group of the crystal with no C_{4h} selection rule breakdown. The phonon modes belong to a continuous frequency range that lies from 0 to 600 cm^{-1}, the highly ionic character of these compounds making it impossible to separate the internal vibrations of a tetrahedral unit from external vibrations. Frequency dependent functions, such as optical indices and absorption coefficient, have been deduced from infrared results. Thanks to the large number (29) of vibrational mode frequencies available through the optical spectroscopies, it has been possible—with a rigid-ion model—to determine the interatomic force constants; the obtained values are consistent with the results obtained by other authors for metal–fluorine interactions; the agreement between the calculated frequencies and the experimental results is better than 7.7%. The most striking feature is the very strong Zn–F force constant (while the corresponding Li–F interaction is rather weak in $LiYF_4$). Some particularly simple relationships between short-range force constants and phonon frequencies have been found. This modelization makes it possible to deduce the phonon dispersion curves, density of states and ultrasonic velocities. The one-phonon density of states shows an intense peak around 410 cm^{-1}, due to many flat phonon branches in this frequency range. The ultrasonic velocities, deduced from the calculated acoustic branches slopes, show that $CaZnF_4$ exhibits greater elastic anisotropies than $LiYF_4$, which may explain the existence in the former and not in the latter of an easy-cleaving direction.

References

[1] Kaminskii A 1990 *Laser Crystals* (Berlin: Springer)
[2] Schulteiss E, Scharmann A and Schwabe D 1986 *Phys. Status Solidi* **138** 465
[3] Cummins H Z 1983 *Light Scattering Near Phase Transitions* ed H Z Cummins and P A Levanyuk (Amsterdam: North-Holland)
Bulou A, Rousseau M and Nouet J 1992 *Key Engineering Materials* vol 68, ed C Boulesteix (Switzerland: Trans Tech) p 133
[4] Salaün S, Fornoni M T, Bulou A, Rousseau M, Simon P and Gesland J Y 1997 *J. Phys.: Condens. Matter* **9** 6941
[5] Salaün S, Bulou A, Rousseau M, Hennion B and Gesland J Y 1997 *J. Phys.: Condens. Matter* **9** 6957

[6] *Landolt–Börnstein New Series* 1973 vol 7 (Berlin: Springer)
[7] Barker A S Jr 1964 *Phys. Rev.* **135** 742
[8] Porto S P S and Scott J F 1967 *Phys. Rev.* **157** 716
[9] Kurosawa T 1961 *J. Phys. Soc. Japan* **16** 1298
[10] Scott J F 1968 *J. Chem. Phys.* **48** 874
[11] Scott J F 1971 *Phys. Rev.* B **4** 1360
[12] Gervais F 1983 *Infrared and Millimeter Waves* vol 8, ed K J Button (New York: Academic) ch 7, p 279
Gervais F 1976 *Solid State Commun.* **18** 191
[13] Born M and Huang K 1954 *Dynamical Theory of Crystal Lattices* (London: Oxford University Press)
[14] Szigeti B 1950 *Proc. R. Soc.* A **204** 51
[15] Salaün S and Rousseau M 1995 *Phys. Rev.* B **51** 15 867
[16] Benoit C and Giordano J 1988 *J. Phys. C: Solid State Phys.* **21** 5209
[17] Rauh H and Geick R 1985 *Phys. Status Solidi* b **127** 55
[18] Lehner N, Rauh H, Strobel K, Geick R, Heger G, Bouillot J, Renker B, Rousseau M and Stirling W G 1982 *J. Phys. C: Solid State Phys.* **15** 6545
[19] Rousseau M, Gesland J Y, Hennion B, Heger G and Renker B 1981 *Solid State Commun.* **38** 45–7
[20] Becher R R, Sangster M J L and Strauch D 1989 *J. Phys.: Condens. Matter* **1** 7801
[21] Foucher P 1989 *PhD Thesis* University of Paris VI
[22] Catlow C R A, Norgett M J and Ross T A 1977 *J. Phys. C: Solid State Phys.* **10** 1627
[23] Watson G W, Parker S C and Wall A 1992 *J. Phys.: Condens. Matter* **4** 2097
[24] Blanchfield P and Saunders G A 1979 *J. Phys. C: Solid State Phys.* **12** 4673
[25] Von Schnering H G, Vu D and Peters K 1983 *Z. Kristallogr.* **165** 305
[26] Farley J M and Saunders G A 1972 *J. Phys. C: Solid State Phys.* **5** 3021